

## Bottleneck effects in the relaxation and photoluminescence of microcavity polaritons

F. Tassone

*Ginzton Laboratory and ERATO Quantum Fluctuation Project, Stanford University, Stanford, California 94305*

C. Piermarocchi, V. Savona, and A. Quattropani

*Institut de Physique Théorique, Ecole Polytechnique Fédérale, CH-1015 Lausanne, Switzerland*

P. Schwendimann

*Defense Procurement and Technology Agency, System Analysis Division, CH-3003 Bern, Switzerland*

(Received 12 May 1997)

A theoretical model for the investigation of the dynamics of microcavity polaritons in the strong-coupling regime is proposed. The resulting photoluminescence dynamics at small angles is studied as a function of the angle of observation, the cavity detuning, the lattice, and the free-carrier temperature. For small detunings, the strong dispersion of the microcavity polaritons at small angles results in a bottleneck relaxation dynamics, similar to the bulk one. However, important differences, related to the reduced dimensionality of the system, are found. In particular, a larger emission from the upper polariton with respect to the lower polariton is found for any temperature. Moreover, a two-lobe angular emission from the lower branch is also expected. In the case of large pump excess energies, when hot carriers are injected into the system, longitudinal-optical-phonon emission has also been considered as a possible polariton formation mechanism, and shown to reduce only partially the effects summarized above. [S0163-1829(97)06036-0]

### I. INTRODUCTION

In an infinite crystal, the interaction between the radiation field and excitons is characterized by translational invariance and thus wave-vector conservation. A single exciton mode couples to a single radiation mode, giving rise to coupled radiation-excitation modes, called polaritons.<sup>1</sup> Polaritons are a strong mixture of the exciton and photon close to the crossing of the dispersion curves of the photon and the exciton. Outside this crossing region, the polariton has either larger exciton content, or larger photon content. We refer to excitonlike and photonlike polaritons depending on the contents of exciton and photon in the mixed modes. Polaritons in the infinite crystal are stationary states, and no phase space is left for the decay via radiative recombination. Therefore they may radiate only through propagation to the crystal surface.<sup>2</sup> Instead, in a quantum well (QW), because of the reduced dimensionality, the translational symmetry of the electronic states is broken along the growth direction, hereafter denoted by  $\mathbf{z}$ . In this case, a two-dimensional (2D) exciton can recombine to a continuum of photon modes with all the possible values of  $k_z$  and a finite radiative recombination rate results.<sup>3</sup> We do not therefore find strong mixture between the exciton and photon as in the bulk case.

In order to realize the two-dimensional analog of the bulk polariton, a planar structure where both the photon and exciton are confined in the normal direction is necessary. Semiconductor microcavities are planar devices in which the electromagnetic field is confined by means of two parallel plane semiconductor mirrors. When a QW is placed inside a microcavity, excitons are coupled to the electromagnetic modes of the dielectric structure. Typical microcavities have a thickness of a few integer multiples of half the photon wave-

length at the exciton resonance frequency. Consequently, an exciton is coupled to a *single* cavity mode according to the in-plane wave-vector conservation. Thus this system constitutes the 2D analogs of the bulk polariton.<sup>4</sup> In microcavities the photons have a finite lifetime which originates from the finite transmittivity of the mirrors. This implies a radiative mechanism for microcavity polaritons which, in contrast to bulk polaritons, does not involve propagation and surface recombination.

One of the major issues in the study of optical properties of bulk polaritons has been the description of the photoluminescence (PL) process, which is the result of the interplay between radiative recombination and energy relaxation through the interaction of excitons with phonons. The relaxation processes and the results of PL measurements have been successfully understood after detailed theoretical investigations of the dynamics of polaritons.<sup>2,5</sup> The effective recombination times in these systems vary by orders of magnitude, being very short for photonlike polaritons, and much longer for excitonlike polaritons. When the interaction with phonons is taken into account, the relaxation times due to phonon scattering become much longer for the photonlike polariton than for the excitonlike polariton. This effect is due to the reduced exciton content in the photonlike polariton and to the increased slope of its dispersion. The combination of the increase of radiative rate and decrease of the relaxation rate in passing from the excitonlike to photonlike modes results in a depletion of polaritons in the photonlike region, and in the absence of any further energy relaxation in this region. This overall dynamics of the 3D polariton has thus been called a bottleneck dynamics.<sup>2</sup> The theoretical description of such effect presents several difficulties. In particular, surface and spatial propagation effects (i.e., the fact that the

polariton density is not uniform in the sample<sup>6</sup>), and elastic scattering from impurities strongly modify the polariton luminescence line.<sup>6,7</sup> The dynamical effect considered above has been observed in the bulk both in continuous-wave<sup>6</sup> and time-resolved experiments.<sup>7,8</sup>

The small exciton binding energy in bulk GaAs makes the bulk polariton weak to both large temperatures and impurity concentration. Therefore, the bottleneck effects are observed only in very pure samples at low temperature. However, these types of dynamics may be more easily observed in a system of reduced dimensionality, like semiconductor microcavities, where the exciton binding energies are increased and the radiative recombination process becomes allowed.<sup>3</sup> In such systems, the impurity luminescence becomes effectively quenched by the fast radiative decay, and the PL dynamics of the polaritons may be observed up to larger temperatures than in the bulk. In the present work, we study the dynamics of microcavity polaritons. Our aim is to understand the fundamental processes underlying the PL, both in stationary and time-resolved regimes, and to understand the similarities and differences with the bulk system. We do, however, consider realistic systems, which present some additional differences with respect to the ideal 2D polariton. Currently, good quality microcavities have been realized in many laboratories.<sup>9–12</sup> Quarter-wavelength stacks of transparent semiconductors, known as distributed Bragg reflectors (DBR's), are used to efficiently confine the light in the cavity.<sup>13</sup> For large angles, however, the reflectivity of the DBR's drops well below unity. Therefore the radiation is not effectively confined at these large angles and leaks out efficiently. Because of the DBR design, this loss takes place through modes which propagate inside the sample substrate, where the radiation is then absorbed. These modes are usually called leaky modes.<sup>4</sup> As a consequence, the realization of the two-dimensional polariton is somewhat partial, being limited to small angles (or small in-plane wave vectors). In a previous paper,<sup>14</sup> we have shown how these characteristics of the DBR influence the *overall* PL dynamics of the microcavity. It was shown that the PL decay time is dominated by the leakage of radiation at large angles, and is close to the one obtained for bare quantum wells. Experimental confirmation of the above theoretical results has been obtained recently.<sup>15</sup> Thus the overall decay dynamics is not of the bottleneck type as for the bulk. However, the emitted luminescence is observed in the region of good mirror reflectivity. We call this angular region the strong-coupling region. In this paper, we study in detail the PL in this strong-coupling region, both in the time-resolved and continuous-wave cases. Some similarities with respect to the bottleneck dynamics taking place in the bulk case are found, such as the depletion of the strongly mixed modes. However, we put into evidence qualitative and quantitative differences between the characteristic resulting PL in the two cases. In particular, we find that the lower polariton peak emission at any temperature and for small exciton-cavity detuning is small compared to the upper polariton one; thus a large deviation from the thermal population of these modes is predicted.

The paper is divided as follows. In Sec. II we briefly summarize the calculation of the polariton modes of a realistic cavity, of their radiative recombination rates, and of the scattering rates by phonons. We set up a rate-equation model

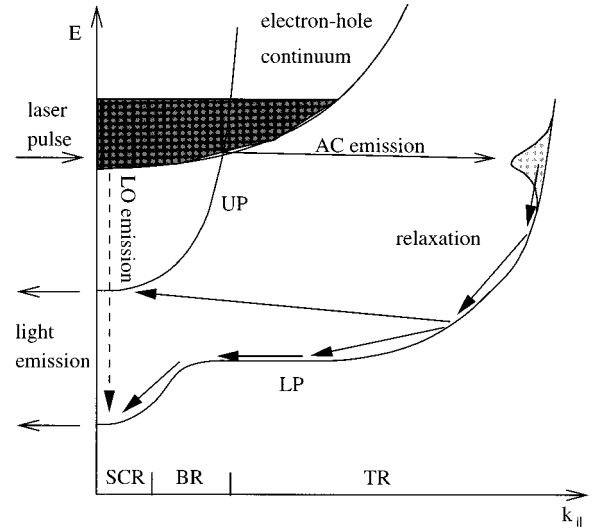


FIG. 1. Schematic representation of the polariton dispersion, the free-carrier thermal reservoir, and the possible polariton formation processes: scattering processes by acoustic-phonon emission or absorption, and radiative recombination. UP: upper branch; LP: lower branch; SR: strong-coupling region; BR: bottleneck region; TR: thermal region.

for the dynamics, and introduce in Sec. III the pump terms for nonresonant excitation. In particular, we calculate the polariton formation rates as functions of the carrier temperature, including the formation process by the emission of optical phonons. In Sec. IV, we first discuss the overall dynamics, and then the detuning dependence of the rise time. In the case of stationary experiments, we study the emission as a function of the lattice temperature, the angle of emission, and the cavity detuning. Finally, in Sec. V the results are discussed with comparisons to available measurements.

## II. RATE-EQUATION MODEL OF THE DYNAMICS AND OF THE PHOTOLUMINESCENCE

We identify three steps in the description of photoluminescence from semiconductors: an excitation provided by an external pump, a relaxation process in which the energy of the excitation is redistributed among the electronic states and released to the lattice, and a radiative recombination process. In general, all these processes are characterized by different time scales. In Fig. 1 we give a schematic picture of the polariton dispersion and of the possible scattering processes governing its dynamics and PL that we are going to consider. These include acoustic-phonon scattering within the polariton branches, polariton formation from a thermal reservoir of free carriers through acoustic- or optical-phonon emission, and polariton radiative recombination. Neglect of other processes like exciton-carrier, exciton-exciton scattering, and exciton dissociation is justified by the range of low lattice temperatures and low carrier densities considered. In the following, we assume that the dynamics of the scattering is well described by a set of rate equations. This semiclassical approximation is justified by the relatively small scattering rates of the polaritons with the phonons and external cavity photons (polariton radiative decay) with respect to the typical changes in the particle energies during the scattering

events. In other words, it is fully justified to neglect the small effects of scattering on the energy dispersion of the particles, e.g., the variation of the exciton-polariton masses and Rabi splitting. This is appropriate for low-density excitation. The rate equations read

$$\begin{aligned} \dot{n}_{i,\mathbf{k}} = & \sum_{j,\mathbf{k}'} W_{j,\mathbf{k}' \rightarrow i,\mathbf{k}} n_{j,\mathbf{k}'} (n_{i,\mathbf{k}} + 1) \\ & - \sum_{j,\mathbf{k}'} W_{i,\mathbf{k} \rightarrow j,\mathbf{k}'} n_{i,\mathbf{k}} (n_{j,\mathbf{k}'} + 1) - \Gamma_{i,\mathbf{k}} n_{i,\mathbf{k}} + F_{i,\mathbf{k}}. \end{aligned} \quad (1)$$

The terms containing  $(n+1)$  correspond to stimulated polariton emission, and are hereon approximated by unity because of the low density considered. Here  $W_{i,\mathbf{k} \rightarrow j,\mathbf{k}'}$  are the polariton scattering rates mediated by the phonons,<sup>14</sup>  $\Gamma_{i,\mathbf{k}}$  is the radiative recombination rate,<sup>4</sup> and the source terms  $F_{i,\mathbf{k}}$  represent the injection of polaritons from the free carriers. These last terms are related to the exciton formation rates calculated in Ref. 16, and their specific expression in the polariton system will be discussed in Sec. III. Dissociation of exciton polaritons into free carriers by absorption or emission of phonons is negligible at the low lattice temperatures considered in this work.

The scattering rates of microcavity polaritons by acoustic phonons  $W_{i,\mathbf{k} \rightarrow j,\mathbf{k}'}$ , where  $\mathbf{k}$  and  $\mathbf{k}'$  are the in-plane microcavity polariton wave vectors, and  $i$  and  $j$  are the branch indexes, are calculated by using the deformation potential interaction and the Fermi golden rule.<sup>14</sup> Emission and absorption of optical phonons within the microcavity polariton bands is impossible, due to the large LO-phonon energy. The scattering rate  $W_{i,\mathbf{k} \rightarrow j,\mathbf{k}'}$  is the sum of two contributions arising from phonon emission and absorption. The Fermi golden rule for the absorption (−) or emission (+) term gives

$$\begin{aligned} W_{i,\mathbf{k} \rightarrow j,\mathbf{k}'}^{\pm} = & \frac{2\pi}{\hbar} \sum_{q_z} |X_{j,\mathbf{k}'}^* \langle \mathbf{k}' | \langle 0_{\mathbf{q},q_z} | H_{\text{exc-ph}} | 1_{\mathbf{q},q_z} \rangle | \mathbf{k} \rangle X_{i,\mathbf{k}}|^2 \\ & \times \delta(\hbar\Omega_{j,\mathbf{k}'} - \hbar\Omega_{i,\mathbf{k}} \pm E_{\mathbf{q},q_z}^{(\text{ph})}) (n_{E_{\mathbf{q},q_z}^{(\text{ph})}} + 1/2 \pm 1/2). \end{aligned} \quad (2)$$

Here  $\mathbf{q} = \mathbf{k}' - \mathbf{k}$  is the exchanged in-plane momentum,  $H_{\text{exc-ph}}$  is the deformation potential interaction,  $|n_{\mathbf{q},q_z}\rangle$  is a phonon number state,  $|\mathbf{k}\rangle$  is the exciton state of wave vector  $\mathbf{k}$ ,  $\hbar\Omega_{i,\mathbf{k}}$  is the polariton energy, branch  $i$ , wave vector  $\mathbf{k}$ ,  $n(E^{(\text{ph})})$  is the Bose occupation number for phonons, and  $E_{\mathbf{q}}^{(\text{ph})} = \hbar u q$  is the phonon energy.  $X_{i,\mathbf{k}}$  are the Hopfield coefficients whose square modulus gives the exciton content in the polariton state of branch  $i$  and wave vector  $\mathbf{k}$ .<sup>14,17</sup> The explicit expression of  $W^{\pm}$  as a function of the conduction- and valence-band deformation potentials  $a_e$  and  $a_h$  is then

$$\begin{aligned} W_{i,\mathbf{k} \rightarrow j,\mathbf{k}'}^{\pm} = & \frac{4\pi}{\hbar} \frac{L_z}{2\pi} \frac{\hbar}{2\rho\mathcal{V}u} \frac{(|\mathbf{k} - \mathbf{k}'|^2 + q_z^{(0)2})}{|\hbar u q_z^{(0)}|} \\ & \times |X_{j,\mathbf{k}'}^* X_{i,\mathbf{k}}|^2 [n(E_{\mathbf{k}' - \mathbf{k}, q_z^{(0)}}^{(\text{ph})}) + 1/2 \pm 1/2] \\ & \times \left[ a_e I^{\parallel} \left( \frac{m_h}{M} |\mathbf{k}' - \mathbf{k}| \right) I_e^{\perp}(q_z^{(0)}) \right. \\ & \left. - a_h I^{\parallel} \left( \frac{m_e}{M} |\mathbf{k}' - \mathbf{k}| \right) I_h^{\perp}(q_z^{(0)}) \right]^2, \end{aligned} \quad (3)$$

where  $q_z^{(0)}$  reads

$$q_z^{(0)} = \left[ \left( \frac{\Omega_{j,\mathbf{k}'} - \Omega_{i,\mathbf{k}}}{u} \right)^2 - |\mathbf{k} - \mathbf{k}'|^2 \right]^{1/2}. \quad (4)$$

Here  $L_z$  is the growth direction quantization size,  $\mathcal{V}$  the quantization volume,  $u$  the speed of the longitudinal acoustic mode, and  $\rho$  the mass density of the solid. The terms  $I^{\parallel}(q)$  and  $I_e^{\perp}(q_z)$  are the superposition integrals of the exciton in-plane wave functions and the phonon waves. We consider the following exciton envelope wave function:

$$\Psi_{\mathbf{k}}(\boldsymbol{\rho}, z_e, z_h) = F_{\mathbf{k}}(\rho) c(z_e) v(z_h), \quad (5)$$

where  $F_{\mathbf{k}}(\rho) = \sqrt{2/\pi a_B^2} \exp(-\rho/a_B)$  is the in-plane exciton envelope function,  $c$  and  $v$  are the electron and hole confinement functions, and  $a_B$  the exciton Bohr radius. Then the superposition integrals read<sup>18</sup>

$$I^{\parallel}(|\mathbf{q}|) = \left( \frac{2}{\pi a_B} \right)^{1/2} \left[ 1 + \left( \frac{q a_B}{2} \right)^2 \right]^{-3/2}, \quad (6)$$

$$I_e^{\perp}(q_z) = \int dz |c(z)|^2 e^{iq_z z}.$$

Expressions analogous to Eq. (6) hold for  $I_h^{\perp}$  with  $m_e$  in place of  $m_h$ , and  $v(z)$  in place of  $c(z)$ . These integrals introduce cutoffs in the scattering with phonons having  $q_{\parallel} > 1/a_B$  or  $q_z > 2\pi/L$  ( $L$  is the QW width), and have been discussed in detail in Ref. 18. In order to calculate the scattering rates, we need to specify the exact energy dispersion  $\Omega_{i,\mathbf{k}}$  of the polariton modes. We use the results which have been presented elsewhere<sup>4</sup> for a GaAs-based realization of a one-wavelength semiconductor microcavity having a single QW embedded at its center. High-reflectivity DBR's consisting of 24 and 20 pairs of quarter-wavelength layers, respectively, enclose the cavity. The exact mixed exciton-cavity modes are calculated analytically by diagonalizing the exciton-photon interaction, where the free electromagnetic modes of the full DBR structure are considered.<sup>4</sup> A Rabi splitting  $\hbar\Omega_R = 4$  meV results for these structures, and is a typically observed splitting for these types of structures.<sup>10</sup> In Fig. 2 we plot the total radiative broadening of the modes  $\Gamma_{i,\mathbf{k}}$  for a detuning  $\delta = 0$ . Radiative lifetimes are in the picosecond range, a value which is also typical of GaAs-based quantum well structures, and has been observed experimentally.<sup>19</sup> The radiative rate vanishes outside the radiative region  $k < k_0 = n_{\text{cav}} \Omega_{\text{exc}}/c$ , where  $n_{\text{cav}}$  is the cavity index of refraction. This explains the increase of the overall PL decay time as a function of temperature in two-dimensional structures, when the excited levels are thermally occupied.<sup>20</sup> In the inset of Fig. 2 we plot  $\Gamma_{i,0}$  as a function of the detuning  $\delta$ . We notice that this is rather large, and is proportional to the cavity photon fraction of the polariton mode, with exception made for excitonlike modes, when  $\delta \gg \hbar\Omega_R$ . In the sequel, we are interested in the dynamics of strongly admixed modes only, and we are going to consider  $\delta \approx \hbar\Omega_R$ , and in particular the four detunings  $0$ ,  $\hbar\Omega_R$ ,  $-\hbar\Omega_R$ , and  $-2\hbar\Omega_R$ . For practical purposes, we have also been using an analytical approximation to the exact dispersion, which neglects details of the dispersion effects in the

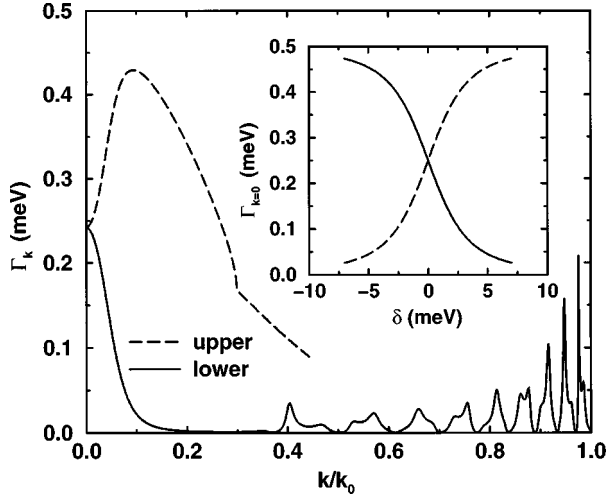


FIG. 2. Microcavity polariton radiative recombination rate  $\Gamma_{\mathbf{k}}$  for a typical GaAs sample considered in this work, at  $\delta=0$ . The inset shows the normal direction radiative recombination rate as a function of the detuning  $\delta$ .

leaky mode region.<sup>4</sup> Its form is given by the usual solutions of the polariton dispersion equations as given in Ref. 21,

$$(\Omega_{\text{exc},\mathbf{k}} - \Omega_{i,\mathbf{k}})(\Omega_{\text{cav},\mathbf{k}} - \Omega_{i,\mathbf{k}}) = \Omega_R^2/4, \quad (7)$$

where  $\Omega_{\text{cav},\mathbf{k}} = \sqrt{c^2/\epsilon_{\text{cav}}\mathbf{k}^2 + \Omega_{\text{cav}}^2}$ . For ease of reference, we also report the expression for the square moduli of the Hopfield coefficients:

$$|X_{i,\mathbf{k}}|^2 = \frac{\Omega_R^2/4}{\Omega_R^2/4 + (\Omega_{i,\mathbf{k}} - \Omega_{\text{exc},\mathbf{k}})^2}. \quad (8)$$

It is instructive to summarize some results on the phonon-scattering rates  $W_{i,\mathbf{k} \rightarrow j,\mathbf{k}'}^\pm$ . In particular, we consider the total phonon-scattering rate, which includes both phonon emission and absorption rates, and is given by

$$\Gamma_{i,\mathbf{k}}^{(\text{ph})} = \sum_{j,\mathbf{k}',l=\pm} W_{i,\mathbf{k} \rightarrow j,\mathbf{k}'}^l.$$

We plot  $\Gamma_{i,\mathbf{k}}^{(\text{ph})}$  in Fig. 3 as a function of energy  $E$  for both the lower and upper branches. We notice its drastic decrease in the strong-coupling region for the lower polariton only. Let us explain in some detail this fundamental point. The acoustic-phonon-scattering rates  $W_{i,\mathbf{k} \rightarrow j,\mathbf{k}'}^l$  are largely quasi-elastic because of the momentum cutoffs shown in Eq. (6). These cutoffs limit exchanged momenta to  $a_B^{-1} = (100 \text{ \AA})^{-1}$  typically for a GaAs QW, where  $L_z \approx a_B$ . The peak exchanged phonon energy is thus close to 1 meV in this case. Therefore, the scattering rate is roughly proportional to the density of states of the polariton modes at the scattering energy. For the lower polariton, interbranch scattering is therefore negligible, and the density of final states is drastically reduced in the strong-coupling region, where the effective polariton mass is orders of magnitude smaller than the exciton mass. For the upper branch instead, interbranch scattering to the lower-branch excitonlike mode is dominant, and consistently much larger scattering rates in the strong-coupling region are obtained. The rapid roll-off of this rate at higher energies is due to the Hopfield factor, i.e., the reduc-

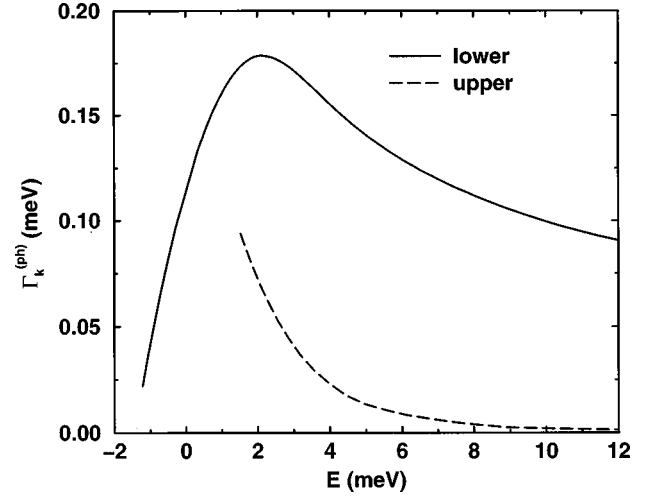


FIG. 3. The total outscattering rates from the lower (solid line) or upper (dashed line) polariton as functions of  $E = \hbar \omega_{\mathbf{k}}$  at a lattice temperature  $T = 30$  K, and at  $\delta = 0$ . The upper-branch scattering is mainly interbranch scattering, while for the lower branch both contributions are shown.

tion of exciton content. This asymmetry between the upper and lower branches for acoustic-phonon scattering is very important in the dynamics, as will be shown later on. The asymmetry is to be traced back to the fact that upper branch polaritons are degenerate with excitonlike modes, whereas lower-branch polaritons in the strong-coupling region are not. This means that this asymmetry is robust to any other elastic-scattering mechanism, and therefore constitutes the dominant feature in the dynamics as long as other strongly non-elastic-scattering mechanisms set in at higher temperatures, or higher densities.

Let us finally discuss how the PL is calculated after the populations resulting from the solution of Eq. (1). We recall that in the strong-coupling regime, the PL spectra consists of two peaks, related to the lower- and upper-branch polariton emissions.<sup>4</sup> The width of these peaks is practically broadened by various effects, but here we are interested in their overall intensity. In the framework of the rate-equation model, summarized in Eq. (1), the PL at a given angle  $\theta$  is proportional to the photon emission rate  $\Gamma_{i,\mathbf{k}} n_{i,\mathbf{k}}$  into the corresponding  $\mathbf{k}$  vector,  $k = n_{\text{cav}} \Omega_{i,\mathbf{k}} / c \sin \theta$ . Here  $n_{\text{cav}}$  is the cavity index of refraction, and  $\theta$  is the propagation angle in the cavity. The propagation angle in air  $\theta_{\text{air}}$  is easily calculated from the relation  $\sin \theta_{\text{air}} / \sin \theta = n_{\text{cav}}$ . Given the large index of refraction of GaAs, we find total internal reflection for most leaky modes. The calculation of the population  $n_{i,\mathbf{k}}$  therefore allows us to calculate the PL emission at any given angle  $\theta_{\text{air}}$  for either the upper or the lower polariton.

### III. NONRESONANT PUMP TERMS

We devote this section to a detailed description of the polariton formation rates from free carriers, as this is an important first step in the dynamics, and may considerably influence the PL. Formation of exciton polaritons may occur through the absorption or emission of acoustic phonons, or through the emission of optical phonons,<sup>16</sup> as schematically shown in Fig. 1. We therefore generically write the formation term as

$$F_{\mathbf{k}} = [C_{\text{ac},\mathbf{k}} + C_{\text{LO},\mathbf{k}}] n_C^2. \quad (9)$$

Here  $n_C$  is the carrier density, and  $C_{\text{ac}}$  and  $C_{\text{LO}}$  are formation coefficients for the acoustic-phonon and optic-phonon formation processes, respectively. It is quite reasonable to assume a thermal distribution for the free carriers, with a given carrier temperature  $T_C$ , which may generally be different from the lattice temperature  $T$ . In fact, fast intracARRIER dynamics is quite effective already at low densities and redistributes the energy among the carriers, so as to produce a thermal distribution.<sup>22</sup> The exchange of acoustic phonons involves energies of the order of less than 1 meV. Thus only lower-branch excitonlike polaritons at the energy-band edge are created by this process, because upper branch polaritons are photonlike at the band edge. We also expect that the memory of the initial distribution of formed excitons is lost during the relaxation on the excitonlike branch. For this reason, we model formation by acoustic-phonon emission or absorption by a simple sharp delta function,

$$C_{\text{ac},\mathbf{k}} \approx C^{(0)} \delta(E_{\text{low},\mathbf{k}} - E_{\text{bind}}),$$

where  $E_{\text{bind}}$  is the exciton binding energy. The formation coefficient has been calculated in Ref. 16, and here we report its expression for ease of reference:

$$C^{(0)} = \left( \frac{2\pi\hbar^2}{k_B T_C} \right)^2 \frac{1}{m_e m_h} \frac{2\pi\hbar^2}{m_{\text{exc}} S} \\ \times \sum_{\mathbf{k}_e, \mathbf{k}_h, \mathbf{k}} \tilde{C}_{\mathbf{k}_e, \mathbf{k}_h \rightarrow \mathbf{k}}^{\text{ac}} e^{-[\hbar^2 \mathbf{k}_e^2 / (2m_e) + \hbar^2 \mathbf{k}_h^2 / (2m_h)] / k_B T_C}, \quad (10)$$

$$\tilde{C}_{\mathbf{k}_e, \mathbf{k}_h \rightarrow \mathbf{k}}^{\text{ac}} = \sum_{l=\pm 1/2} \frac{4\pi}{\hbar} \frac{L_z}{2\pi} \frac{\hbar}{2\rho\mathcal{V}u} \frac{(|\mathbf{k} - \mathbf{k}_e - \mathbf{k}_h|^2 + q_z^{(0)2})}{|\hbar u q_z^{(0)}|} \\ \times [n(E_{\mathbf{k}_e + \mathbf{k}_h - \mathbf{k}, q_z^{(0)})}^{(\text{ph})} + 1/2 + l] \frac{8\pi a_B^2}{S} \\ \times \left[ a_e I^{\parallel} \left( 2 \left| \mathbf{k}_h - \frac{m_h}{M} \mathbf{k} \right| \right) I_e^{\perp}(q_z^{(0)}) \right. \\ \left. - a_h I^{\parallel} \left( 2 \left| \mathbf{k}_e + \frac{m_e}{M} \mathbf{k} \right| \right) I_h^{\perp}(q_z^{(0)}) \right]^2.$$

Here all the constants and expressions have already been introduced for the phonon-scattering-rates, Eq. (3). Concerning optical-phonon emission, it is clearly not quasielastic due to the large, dispersionless energy of the optical phonon. Thus both lower- and upper-branch polaritons are formed by this process. The expression for  $C_{\text{LO}}$  is similar to the one given above for the acoustic phonon, provided the deformation potential interaction is replaced by the Fröhlich interaction, and the appropriate Hopfield factors for exciton content in the final state are included. These formation rates have also been calculated in Ref. 16 for the exciton. Here we include the Hopfield factors, and report the full expression

$$C_{\text{LO},j,\mathbf{k}} = \left( \frac{2\pi\hbar^2}{k_B T_C} \right)^2 \frac{1}{m_e m_h} \sum_{\mathbf{k}_e, \mathbf{k}_h} \tilde{C}_{\mathbf{k}_e, \mathbf{k}_h \rightarrow j, \mathbf{k}}^{\text{LO}} \\ \times e^{-[\hbar^2 \mathbf{k}_e^2 / (2m_e) + \hbar^2 \mathbf{k}_h^2 / (2m_h)] / k_B T_C},$$

$$\tilde{C}_{\mathbf{k}_e, \mathbf{k}_h \rightarrow j, \mathbf{k}}^{\text{LO}} = \sum_{q_z} \frac{2\pi}{\hbar} \frac{\hbar \omega_{\text{LO}} e^2 (1/\epsilon_{\infty} - 1/\epsilon_0)}{\mathcal{V}(|\mathbf{k} - \mathbf{k}_e - \mathbf{k}_h|^2 + q_z^2)} \frac{8\pi a_B^2}{S} \\ \times [1 + n_{\text{LO}}(T_C)] |X_{j,\mathbf{k}}|^2 \left[ I^{\parallel} \left( 2 \left| \mathbf{k}_h - \frac{m_h}{M} \mathbf{k} \right| \right) I_e^{\perp}(q_z) \right. \\ \left. - I^{\parallel} \left( 2 \left| \mathbf{k}_e + \frac{m_e}{M} \mathbf{k} \right| \right) I_h^{\perp}(q_z) \right]^2 \\ \times \delta \left( \frac{\hbar^2 \mathbf{k}_e^2}{2m_e} + \frac{\hbar^2 \mathbf{k}_h^2}{2m_h} - \hbar \omega_{\text{LO}} - \frac{\hbar^2 \mathbf{k}^2}{2M} - E_{\text{bind}} \right). \quad (11)$$

Here the low- and high-frequency dielectric functions  $\epsilon_0$  and  $\epsilon_{\infty}$  define the Fröhlich interaction in the usual way. We notice the fact that the LO phonon is dispersionless, therefore the distribution in energy of the injected polaritons mirrors that of the free carriers times the Hopfield factor. The Hopfield factors are less than one in the strong-coupling region. It is therefore important to consider them even in the pump terms.

Concerning the carrier temperature  $T_C$ , it is a function of both the excess pump energy and of the lattice temperature  $T$ . In this paper we are not interested in the detailed dynamics of the carrier temperature, which we are going to report elsewhere. We are instead interested in the stationary PL, where a stationary  $T_C$  is also established. Both acoustic and LO phonons contribute to the cooling (or heating) of the free-carrier distribution. Since the LO phonons become very effective for  $T > 60$  K in GaAs, it is only in this range that the carrier temperature  $T_C$  is necessarily close to  $T$ . Some small deviations may be expected for very large excess energies (i.e., in the tens of meV range). For lower lattice temperatures  $T$ , which is the case considered here,  $T_C$  may be substantially different from the lattice temperature. However, it is unlikely for  $T_C$  to be far above 60 K for GaAs, because the LO-phonon emission rapidly cools down the free carriers in such a case. The largest  $T_C$  we will consider is therefore 60 K. From the results of Ref. 16, it follows that the total formation rate by acoustic phonons  $C^{(0)}$  is weakly dependent on  $T_C$ , whereas the total formation rate by LO-phonon emission  $\sum_k C_{\text{LO},k}$  is exponentially dependent on  $T_C$ , like  $e^{-(\hbar \omega_{\text{LO}} - E_{\text{bind}}) / k_B T_C}$ . The crossover temperature is around 40 K. We therefore consider only the case  $T_C = 60$  K for dominant LO formation processes, or  $T_C$  below 40 K for dominant acoustic-phonon-mediated formation, leaving aside the crossover region where both processes have to be considered at the same time. In Fig. 4 we present the polariton formation coefficient  $C_{\text{LO},j,\mathbf{k}}$  as a function of the energy of the created polariton for  $T_C = 60$  K. We notice that in the strong-coupling region the coefficient follows the variation of the Hopfield coefficient. Therefore the upper polariton formation coefficient is rapidly cut off at high energies. On the excitonlike lower branch the formation coefficient simply shows the Boltzmann tail at the free-carrier temperature  $T_C$  (a temperature of 60 K is equivalent to an energy of about 6 meV). This calculation also shows that although the formation rate is reduced in the strong-coupling region by the presence of the Hopfield factor, it still remains sizable. Thus lower-branch polaritons in the strong-coupling region are

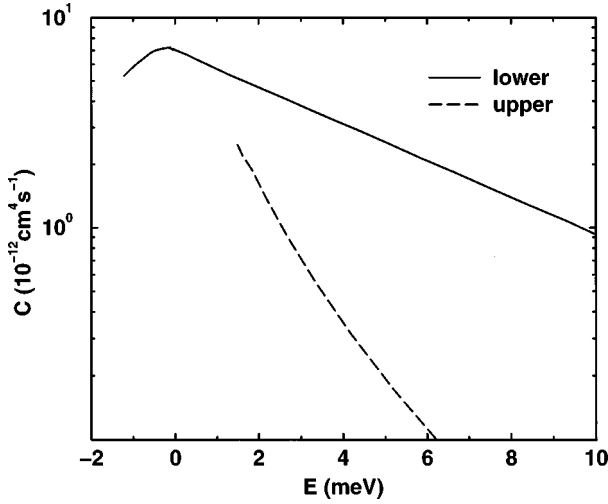


FIG. 4. The lower branch (solid line) and upper branch (dashed line) polariton LO-phonon formation rates as a function of the polariton energy (the origin is fixed at the exciton energy), at a carrier temperature  $T_C = 60$  K.

likely to be directly injected by LO-phonon emission, while it is unlikely for them to be injected by intrabranch acoustic-phonon scattering. Qualitative changes in the dynamics and in the PL are thus expected for large  $T_C$ .

#### IV. PHOTOLUMINESCENCE IN THE STRONG-COUPLING REGION

##### A. Dynamics

The overall microcavity polariton dynamics and, in particular, the decay time of both branches, and the rise time of the lower branch PL, have already been discussed in Ref. 14. We recall here that the strong-coupling region spans a small portion of the  $\mathbf{k}$  space with respect to the whole exciton branch. Moreover, radiative recombination in the excitonlike branch is still present despite of the cavity confinement of radiation, due to the existence of leaky modes in the mirrors. Thus, the total population decay rate and, consequently, the PL decay time, are uniquely determined by the dynamics within the excitonlike branch.<sup>23</sup>

We now discuss in detail the dynamics of the lower- and upper-branch PL rise times separately. We remark that the rise time has been defined as the time necessary for the PL signal to reach its maximum. We have shown in Ref. 14 that the lower branch PL rise time is detuning independent. We first notice that in a first step of the relaxation, the excitons cool down to the bottom of the excitonlike branch by phonon emission. At this point a bottleneck in further relaxation into the strong-coupling region is produced, as for the bulk. This is always caused by a combination of the slowdown of relaxation rates into this region, and increased radiative recombination rates. The question arises of how PL at the bottom of the lower polariton branch,  $\mathbf{k}=0$ , is produced. From the above discussion, we may exclude a cascade involving multiple phonon emission in the relaxation to  $\mathbf{k}=0$ . Instead, relaxation involves a single jump with a single-phonon emission, as shown in Fig. 1. A rather large amount of energy is then released during relaxation to the phonon. This is in apparent contrast to the claimed quasielasticity in the scattering

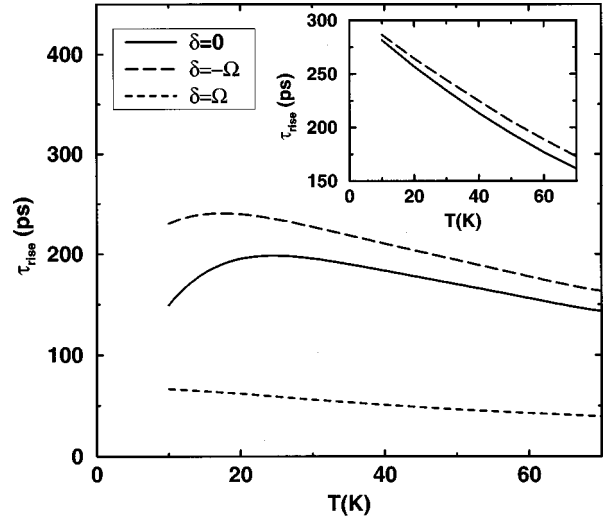


FIG. 5. Rise time  $\tau_R$  as a function of the lattice temperature for the upper-branch PL. Three different detunings are considered. The inset show the rise time for the lower polariton branch. Here the  $\delta = -\Omega$  case coincides practically with the  $\delta = \Omega$  case, and it is not reported in the figure.

of polaritons with phonons. However, it results from the calculations that the energy exchanged in the scattering process is *peaked* around 1 meV, but still displays long tails around this value. The broadening of this energy distribution is both determined by the cutoffs in the superposition integrals (6) and by the shape of the phonon population factor  $n(E)$ , into which the temperature dependence enters. As a consequence, we understand that the rate for scattering from the bottleneck region to the bottom of the lower polariton branch is very small, though finite (see Fig. 1). In particular, we remark that the narrower the distribution of the exchanged energy, the smaller this rate is going to be. Clearly, the radiative rate  $\Gamma_{\text{low}, \mathbf{k}=0}$  is much larger than this rate at which the  $\mathbf{k}=0$  mode is populated. Thus, by inspection of Eq. (1), we understand that  $n_{\text{low}, \mathbf{k}=0}$  adiabatically follows the population at the bottom of the excitonlike branch. We conclude that the rise time of the PL at  $\mathbf{k}=0$  corresponds to the population buildup time at the bottom of the excitonlike branch, and is only determined by this relaxation time. Hence it is detuning independent.

The upper branch PL dynamics differs from the lower branch one in which, at least for the rise time, there is a marked dependence on the detuning. In particular, in Fig. 5, we see that the rise time decreases with increasing positive detuning. To explain this behavior we remark that the only mechanism for the population of the upper branch is interbranch scattering from excitons in the lower branch. In fact, we already noticed that upper-branch polaritons at the electron-hole continuum energy are unlikely to be formed because of their small exciton content. The interbranch scattering is quasielastic, always in the sense explained in detail above. Then, mostly excitons in a portion of the lower branch having the same energy as the bottom of the upper branch are involved in this interbranch scattering process. These ‘‘horizontal’’ scattering processes are shown in Fig. 1, and are allowed by the degeneracy in energy of the upper branch and the excitonlike branch. It also happens that even in this case  $\Gamma_{\text{up}, \mathbf{k}=0}$  is larger than this populating rate. We

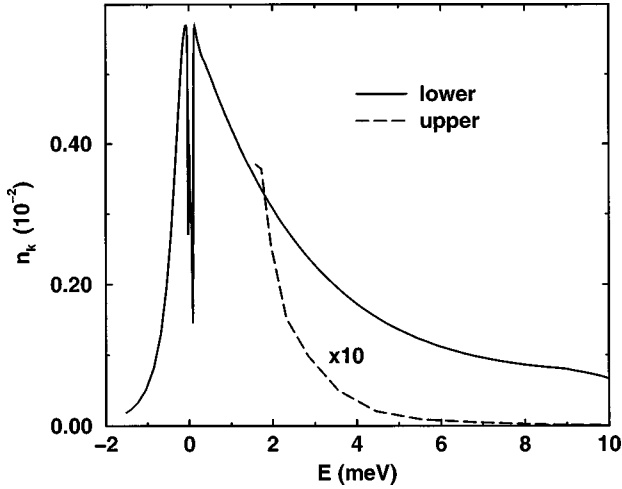


FIG. 6. The stationary population of the lower- and upper-branch polaritons at  $\delta=0$ , and at  $T=30$  K.

conclude that the population  $n_{\text{up},\mathbf{k}=0}$  adiabatically follows the population of the excitonlike branch at the same energy. The first remark, that the upper-branch rise time is usually shorter than the lower-branch one, thus finds an obvious explanation. In fact, cooling excitons reach these higher energies well before reaching the bottom of the excitonlike band. The other remark, that this rise time depends markedly on the detuning, as is shown in Fig. 5, is also clearly explained, as for larger positive detunings the energy of the  $\mathbf{k}=0$  upper-branch polariton is also higher. On the opposite side of detunings, the upper branch becomes excitonlike; thus the PL rise time approaches the value found for the lower branch, as appears in Fig. 5.

### B. Stationary photoluminescence

The stationary solutions of the rate equations (1) for continuous wave pump are obtained by setting  $dn/dt=0$ . The resulting populations for the case of low free-carrier temperature (formation assisted by acoustic phonons) and  $T=30$  K is shown in Fig. 6. The strong-coupling region (few meV around zero energy, labeled by SR in Fig. 1) is depleted for both the upper and lower branches with respect to the excitonlike branch. The population in the excitonlike branch is instead quasithermal (labeled TR in Fig. 1), apart from small deviations in the radiative region.<sup>24</sup> This picture is clearly consistent with the interpretation of the polariton dynamics given in Sec. IV A above. The depletion with respect to the thermal distribution is a consequence of the large radiative recombination rates in the strong-coupling region, as compared with the relaxation rates. Moreover, the decrease of the relaxation rates in the strong-coupling region for the lower branch represents a typical bottleneck in the local dynamics of the system (i.e., in the strong-coupling region only, but not for the overall decay dynamics governed by the leakage through the leaky modes). All these results are thus similar to those which are found in the bottleneck dynamics in the bulk.<sup>2</sup> As for the consequences in the PL, some important differences have to be remarked upon. First, in the selection rules for the PL emitted from a microcavity, there is a one-to-one correspondence between the angle of detection and the in-plane polariton wave vector. For a given ob-

servation angle, only two polariton peaks appear in the spectrum. On the other hand, in the bulk the three-dimensional polariton wave vector is conserved until the polariton reaches the surface. At this point, the component orthogonal to the surface is not conserved for the outgoing photon. Thus, in the bulk, the PL at a given angle is the result of the contribution of polaritons with all the possible values of the wave vector, and it is very difficult to relate the resulting PL line shape to the polariton dispersion and the polariton distribution function at the sample surface. As a consequence, the angular-resolved PL gives information on the dispersion only in the 2D case. Second, in two dimensions the strength of the coupling to the external photons is tuned by the cavity mirror reflectivity. For the semiconductor surface, coupling is a given parameter and is not easily changed. Third, in the cavity case, the exciton and photon fraction of the modes are easily changed by varying the detuning  $\delta$ , which is not possible in three dimensions. Because of all these features, the PL from 2D systems provides more information on the inner processes than in the 3D case. In particular, the PL may be accurately studied as a function of two measurable parameters: the angle and the cavity detuning. As a further limitation in the interpretation of the experimental results, the polariton spectrum in three dimensions is dominated by impurity emission, and most of the studies have only shown lower-branch emission and used LO-phonon replicas to study the occupations in this branch. Therefore, the cavity systems represent a unique workbench where the polariton dynamics can be accurately studied. In Fig. 7 we plot the emission from the upper (a) and lower (b) branches at normal incidence as functions of the lattice temperature  $T$ , and for different detunings. We only consider exciton formation assisted by acoustic phonons, which is the case for small excess energy excitation of the system. The emission from the upper branch is overwhelming, and rapidly increases with temperature. The lower-branch emission remains instead fairly constant as a function of temperature. These two facts are explained as follows, by also keeping in mind the results of Sec. III. The population in the excitonlike part of the lower polariton branch is quasithermal, and can be parametrized as

$$n_{\mathbf{k}} \propto \frac{2\pi\hbar^2}{Mk_B T} e^{-(\hbar^2\mathbf{k}^2/2M)/k_B T}.$$

All the constants have been introduced before. We then consider the rate equations (1) in the stationary case and for  $\mathbf{k}=0$ , and remark that the fast radiative rate means  $\Gamma_{i,\mathbf{k}=0} \gg \sum_{j,\mathbf{k}'} W_{j,\mathbf{k} \rightarrow i,\mathbf{k}'} = \Gamma_{i,\mathbf{k}}^{(\text{ph})}$ . Moreover, we have shown that, for this same reason, most of the polariton population is within the excitonlike part of the lower branch, as seen in Fig. 6. Thus the PL becomes simply

$$I_{i,\mathbf{k}=0} \propto \sum_{j,\mathbf{k}'} W_{j,\mathbf{k} \rightarrow i,\mathbf{k}'} \frac{2\pi\hbar^2}{Mk_B T} e^{-(\hbar^2\mathbf{k}^2/2M)/k_B T}.$$

We call this kind of dynamics a two-step process because the inverse scattering process from  $\mathbf{k}=0$  to the other  $\mathbf{k}$  vectors is negligible. It is essentially the stationary process corresponding to the rise-time process of the lower branch explained in detail in Sec. IV A. When we consider Eq. (3) for the phonon-scattering rates, and the fact that the Bose occupa-

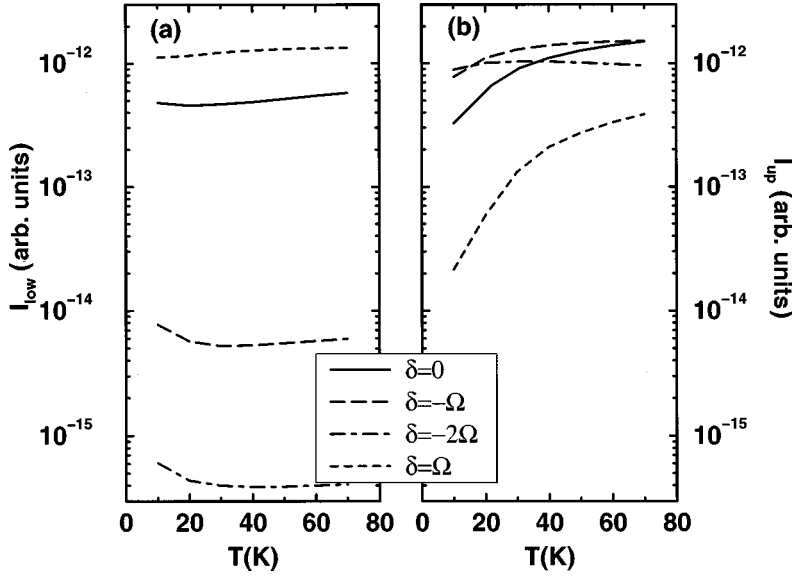


FIG. 7. The normal-incidence PL emission from the lower (a) and upper (b) branches as functions of the lattice temperature  $T$  for different detunings  $\delta$ .

tion factor for phonons  $n(E)$  becomes linear in  $k_B T$  when  $k_B T > E$ , we understand that for the lower branch, for temperatures  $k_B T > (\Omega_{\text{exc}, k=0} - \Omega_{\text{low}, k=0})/2$ , the PL signal becomes roughly constant as a function of  $T$ , due to the cancellation of the dependences of the phonon-scattering rates and of the excitonlike population on  $T$ . The detuning dependence for the lower branch shows that the phonon-scattering rates for small or negative detunings are very small, and are decreasing for larger  $|\delta|$ . This is consistent with the observation made in Sec. IV A for these rates. For positive detunings, the lower branch is essentially excitonlike even at  $k=0$ , and the phonon coupling is larger, allowing for a stronger PL signal.

Scattering from the quasithermal exciton reservoir toward the upper branch is mostly quasielastic, thus the scattering rates are always roughly linearly increasing with  $T$ , and

$$I_{\text{up}, k=0} \propto T \frac{2\pi\hbar^2}{Mk_B T} e^{-(\Omega_{\text{up}} - \Omega_{\text{exc}, k=0})/k_B T},$$

where the  $T$  factor comes from the phonon-scattering efficiency. This simple expression thus explains the strong dependence on temperature and detuning of the luminescence from the upper branch as mainly originating from the Boltzmann exponential of the population in the excitonlike part of the polariton dispersion.

In Fig. 8 we show the angular-resolved PL emission from the upper and lower branches, for zero detuning and at a fixed temperature of 30 K. A ‘‘hole’’ in the emission of the lower branch at small angles is evidenced. This is again related to the depletion of the population in the strong-coupling region: the bottleneck effect. This suggests that an angle- and energy-resolved experiment would result in the observation of a two-lobe emission pattern for the lower polariton. Such an effect is even more pronounced for negative detunings  $\delta$ , whereas it of course disappears in the positive detuning case when the lower branch becomes completely excitonlike. The upper-branch emission does not show such a lobe structure.

The above results change significantly when the LO-phonon formation of the polariton is considered. In Fig. 9 we show the emission in the normal direction for a free-carrier

temperature  $T_C = 60$  K, and  $T = 20$  K, as a function of the detuning  $\delta$ . This situation is typical of high excess pump energy at a low lattice temperature, as explained in Sec. III. In this case, part of the formation process consists of a direct polariton formation in the strong-coupling region. We also report the emission in the case of low  $T_C$ , when direct polariton formation is instead negligible, and polaritons are injected at the band edge. It is clear from Fig. 9, that the upper branch emission is scarcely influenced by the direct LO-phonon-mediated formation of polaritons. By inspection of the results for the population distribution, we have established that quasithermalization of the excitonlike polaritons at the lattice temperature  $T$  is also achieved in the case here considered. This is simply due to the fact that the total injection rate by LO-phonon emission [which is established through Eq. (9) and by choosing a stationary carrier density much smaller than  $10^{10} \text{ cm}^{-2}$ ] is in this case much slower than the relaxation rate in the excitonlike branch. Therefore, the luminescence from the upper branch principally origi-

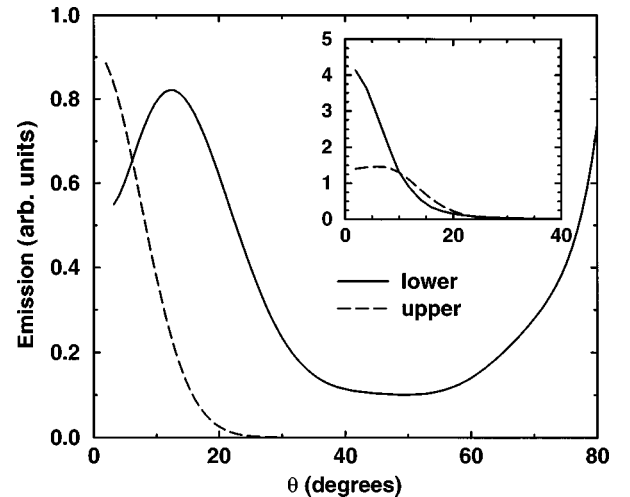


FIG. 8. Angular-resolved PL emission from the lower (solid line) and upper (dashed line) polaritons at zero detuning and  $T = 30$  K. The inset shows the emission of thermalized polaritons for reference.

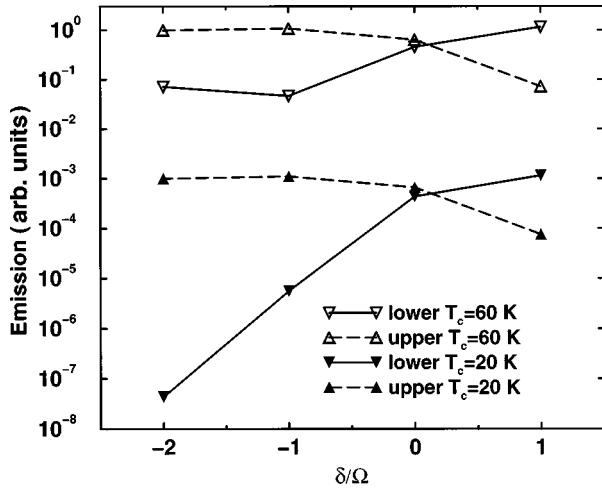


FIG. 9. The normal-incidence PL emission from the lower and upper branches as function of the detuning  $\delta$  for the case of LO-phonon-mediated polariton formation.

rates from interbranch scattering from a quasithermal population of excitons at temperature  $T$ , as in the low- $T_C$  case. The emission from the lower branch is instead greatly influenced by the direct formation of polaritons by LO-phonon emission for zero or negative detunings. In fact, in this case the intrabranch scattering mediated by acoustic phonons, as explained in Sec. II, is extremely inefficient and therefore largely overwhelmed by the direct formation process. As for the strong detuning dependence, we remarked in Sec. III that the formation coefficient depends both on the carrier distribution  $e^{-E/k_B T_C}$  and on the Hopfield factor. Clearly, the exponential increase in the former factor largely compensates for the roughly  $E^{-1}$  decrease [see Eq. (8)] of the latter as the system moves to larger negative detunings. Concerning the angular dependence of the emission, the hole at small angles which was found in the low- $T_C$  case before is effectively reduced by the LO-phonon contribution to the PL at negative detunings. We show in Fig. 10 the lower-branch emission at  $T_C=20$  and 60 K for  $\delta=-2\Omega_R$ . Although an increase in the emission by some orders of magnitude is found for

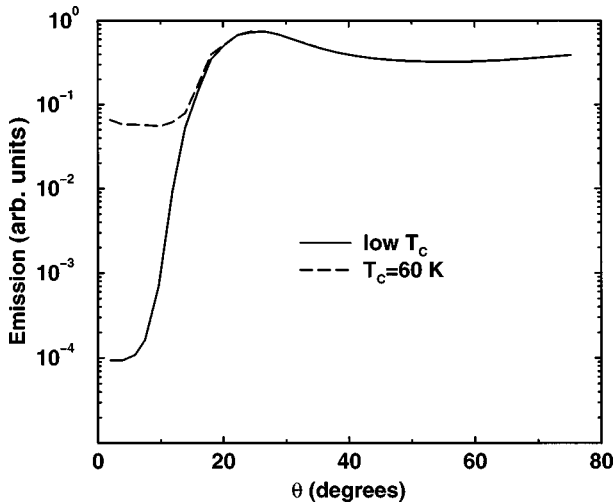


FIG. 10. Angular-resolved PL emission from the lower polariton at zero detuning for  $T_C=60$  K (dashed line) and low  $T_C$  (solid line).

$T_C=60$  K, the strongest emission is still at larger angles, a clear fingerprint of the bottleneck effect. For zero or positive detunings, the direct formation is not equally effective, as clearly appears from Fig. 9, and the hole pattern in the angular emission remains therefore practically unchanged.

## V. DISCUSSION AND CONCLUSIONS

We have shown that the PL emission from a microcavity polariton has a rich phenomenology, and that the simple picture of PL from a thermalized polariton distribution is fundamentally incorrect. In particular, we have shown that it is quite difficult to populate the polaritons in the strong-coupling region. This is a bottleneck effect, similar to that found in the bulk. Luminescence from both the upper- and lower-branch results from one-phonon scattering events from the excitonlike thermally populated reservoir. However, even though the origin of the bottleneck effect is similar in both 2D and 3D systems, the resulting PL is considerably different. As an example, in the microcavity, we find that polariton emission mainly originates from the upper branch at low lattice temperatures. In the bulk, it is even difficult to distinguish between PL from the lower and the upper branch. In fact, we have already remarked in Sec. IV that the selection rules for the polariton radiative recombination are of completely different nature in bulk and microcavity systems. In the first case, in fact, the 3D wave vector is the correct quantum number to describe the polariton state, but is not conserved in the recombination at the sample surface. Conversely, in the microcavity, the 2D in-plane wave which is the quantum number for 2D polaritons, is conserved in the recombination process. Consequently, an angle-resolved experiment allows the observation of the polariton dispersion in a microcavity,<sup>11</sup> while it provides no information on the distribution along the polariton dispersion in the bulk case. We have calculated the angular dependence of the PL from a microcavity. A sharp single-lobe emission over a few degrees is found for the upper branch, but a two-lobe, conically shaped emission is found for the lower branch. This is a main signature of the bottleneck dynamics, and no analog of this angular emission exists for the bulk. We also considered the effects of the injection of carriers at large carrier temperatures, which are obtained with relatively large excess pump energy. The direct creation of polaritons in the strong-coupling region, due to LO-phonon emission, in this case partially reduces the bottleneck effect, and sizably increases the emission from the lower branch at small angles. At large lattice temperature, above 60 K, dissociation by LO-phonon absorption rapidly thermalizes the polaritons, and the usual result of a thermal ratio between the emission of the upper and lower polariton is thus expected. Moreover, an overall sizable increase of the emission of both the modes results, which is related to the disappearance of the bottleneck effect.

Effects of disorder are also different in the bulk and microcavity system, due to their different origin. Impurity centers in the bulk act as trapping centers, effectively quenching the radiative recombination from bulk polaritons.<sup>2,7</sup> Moreover, strong elastic scattering at the transverse exciton energy produces a characteristic dip in the free polariton luminescence.<sup>7</sup> These effects are reduced in the QW, and

surface roughness is instead the dominant scattering mechanism. It does not, however, produce quenching of the radiative recombination, but rather a spectral redistribution of the absorption over a large emission line. Moreover, breaking of the in-plane translation symmetry is presumably a large effect in this case. We have shown that the bottleneck effect and its consequences are intimately related to the translational symmetry. A detailed study of the dynamics in this case is necessary in order to establish whether the bottleneck effect disappears with strong disorder. Indeed, recent PL measurements on microcavity polariton<sup>11</sup> did not explicitly show any evidence of nonthermalized emission in the PL, even when carried out at low lattice temperatures of 30 K.<sup>25</sup> Even though the polariton PL spectra have been measured at different emission angles,<sup>11</sup> the angular dependence of the PL intensity has not been determined. We do not expect to find any trace of the two-lobe emission from the lower branch in these samples in which disorder is quite large, and the polariton broadening amounts to a sizable fraction of the

Rabi splitting. Angular dispersion effects, as well as the other bottleneck effects, are presumably washed out in these samples. Unfortunately, it is not easy to relate the size of the  $k$  mixing with inhomogeneous broadening. Recent theoretical results<sup>26</sup> suggest that, for the lower-branch polariton only, both the inhomogeneous broadening and the  $k$  mixing are effectively reduced for small disorders due to a motional narrowing effect. Thus we expect that the effects predicted in this paper should be detected within a sizable range of disorder. In this linewidth regime, we expect that both a decrease of the lower-branch emission, and the two-lobe emission should indeed be observed.

#### ACKNOWLEDGMENTS

F.T. acknowledges support from the Swiss Optics Priority Program, C.P. from the Swiss National Foundation. Useful discussions with R. P. Stanley, J. Wainstain, and R. Houdré are gratefully acknowledged.

<sup>1</sup>J. J. Hopfield, Phys. Rev. **112**, 1555 (1958).

<sup>2</sup>Y. Toyozawa, Prog. Theor. Phys. Suppl. **12**, 111 (1959).

<sup>3</sup>V. M. Agranovich and A. O. Dubowskii, Pis'ma Zh. Eksp. Teor. Fiz. **3**, 345 (1966) [JETP Lett. **3**, 233 (1966)].

<sup>4</sup>V. Savona, F. Tassone, C. Piermarocchi, A. Quattropani, and P. Schwendimann, Phys. Rev. B **53**, 13 051 (1996).

<sup>5</sup>H. Sumi, J. Phys. Soc. Jpn. **21**, 1936 (1975); W. J. Rappel, L. F. Feiner, and M. F. H. Schuurmans, Phys. Rev. B **38**, 7874 (1988).

<sup>6</sup>C. Weisbuch and R. Ulbrich, J. Lumin. **18/19**, 27 (1979), and references therein.

<sup>7</sup>D. E. Cooper and P. R. Newman, Phys. Rev. B **39**, 7431 (1989).

<sup>8</sup>F. Askary and P. Y. Yu, Phys. Rev. B **31**, 6643 (1985); P. Wiesner and U. Hein, *ibid.* **11**, 3071 (1975); G. W. 't Hooft, W. A. J. A. van der Pöel, L. W. Molenkamp, and C. T. Foxon, *ibid.* **35**, 8281 (1987).

<sup>9</sup>H. Yokoyama, K. Nishi, T. Anan, H. Yamada, S. D. Bronson, and E. P. Ippen, Appl. Phys. Lett. **57**, 2814 (1990).

<sup>10</sup>C. Weisbuch, M. Nishiokam, A. Ishikawa, and Y. Arakawa, Phys. Rev. Lett. **69**, 3314 (1992); T. A. Fisher, A. M. Afshar, D. M. Whittaker, M. S. Skolnick, J. S. Roberts, G. Hill, and M. A. Pate, Phys. Rev. B **51**, 2600 (1995); I. Abram, S. Iung, R. Kuszelewicz, G. LeRoux, C. Licoppe, J. L. Oudar, E. V. K. Rao, J. Bloch, R. Planel, and V. Thierry-Mieg, Appl. Phys. Lett. **65**, 2516 (1994); H. Cao *et al.*, *ibid.* **66**, 1107 (1995).

<sup>11</sup>R. Houdré, C. Weisbuch, R. P. Stanley, U. Oesterle, P. Pellandini, and M. Ilegems, Phys. Rev. Lett. **73**, 2043 (1994).

<sup>12</sup>A. Tredicucci *et al.*, Phys. Rev. Lett. **75**, 3906 (1995).

<sup>13</sup>H. A. McLeod, *Thin-Film Optical Filters*, 2nd ed. (Hilger, Bristol, 1986).

<sup>14</sup>F. Tassone, C. Piermarocchi, V. Savona, A. Quattropani, and P. Schwendimann, Phys. Rev. B **53**, R7642 (1996).

<sup>15</sup>J. Wainstain *et al.*, Superlattices Microstruct. (to be published).

<sup>16</sup>C. Piermarocchi, F. Tassone, V. Savona, A. Quattropani, and P. Schwendimann, Phys. Rev. B **55**, 1333 (1997).

<sup>17</sup>S. Pau, G. Bjork, J. Jacobson, Hui Cao, and Y. Yamamoto, Phys. Rev. B **51**, 7090 (1995).

<sup>18</sup>C. Piermarocchi, F. Tassone, V. Savona, A. Quattropani, and P. Schwendimann, Phys. Rev. B **53**, 15 834 (1996).

<sup>19</sup>B. Sermage, S. Long, I. Abram, J. Y. Marzin, J. Bloch, R. Planel, and V. Thierry-Mieg, Phys. Rev. B **53**, 16 516 (1996).

<sup>20</sup>L. C. Andreani, F. Tassone, and F. Bassani, Solid State Commun. **77**, 641 (1991).

<sup>21</sup>V. Savona, L. C. Andreani, A. Quattropani, and P. Schwendimann, Solid State Commun. **93**, 733 (1995).

<sup>22</sup>W. H. Knox, in *Hot Carriers in Semiconductor Nanostructures*, edited by J. Shah (Academic, San Diego, 1992), p. 313.

<sup>23</sup>This is at difference with the bulk, where the excitonlike modes are weakly coupled to external photons at the surface, and the overall decay time is therefore mainly determined by the bottleneck dynamics explained in Sec. I.

<sup>24</sup>This effect have been studied in detail in Ref. 18, and shown to produce a fixed positive shift in the decay times.

<sup>25</sup>There is, however, evidence of a nonthermalized emission from microcavities for some samples below 30 K [R. P. Stanley, S. Pau, U. Oesterle, R. Houdré, and M. Ilegems, Phys. Rev. B **55**, R4867 (1997)].

<sup>26</sup>V. Savona, C. Piermarocchi, A. Quattropani, F. Tassone, and P. Schwendimann, Phys. Rev. Lett. **78**, 4470 (1997).